A COMPARATIVE STUDY BETWEEN FIELD ORIENTED CONTROL STRATEGY AND DIRECT POWER CONTROL STRATEGY FOR DFIG

Y. DJERIRI*, A. MEROUFEL, A. MASSOUM, and Z. BOUDJEMA

Department of Electrical Engineering, University Djillali Liabes of Sidi Bel Abbes, Algeria, 22000
Intelligent Control and Electrical Power Systems –ICEPS- Laboratory
*djeriri_youcef@yahoo.fr

Abstract: *This paper presents a comparative study of field oriented control (FOC) and direct power control (DPC) strategies in order to control the active and reactive stator powers of a doubly fed induction generator (DFIG), which is applied to wind energy conversion systems (WECS). Traditionally the FOC is achieved by using of classical Proportional-Integral (PI) controller. However this controller depends highly on parameter variations of the DFIG. The proposed DPC strategy produces a fast and robust power response. Simulation results on a 1.5 MW DFIG system are provided to demonstrate the effectiveness and robustness of the proposed control strategy during variations of active and reactive power, rotor speed, and machine parameters.*

Key words: *Doubly Fed Induction Generator (DFIG), Field Oriented Control (FOC), Direct Power Control (DPC).*

1. Introduction

Since fifteen years, the concept of the variable speed wind turbine (VSWT) equipped with a doubly fed induction generator (DFIG) has received increasing attention due to its noticeable advantages over other wind turbine concepts [1-2]. In the DFIG concept, the stator is usually connected directly to the three-phase grid; the rotor is also connected to the grid but via a transformer and two back-to-back converters (Fig. 1). Usually, the rotor-side converter controls the active and reactive power and the grid side converter controls the DC-link voltage and ensures operation of the converter at a unity power factor [1].

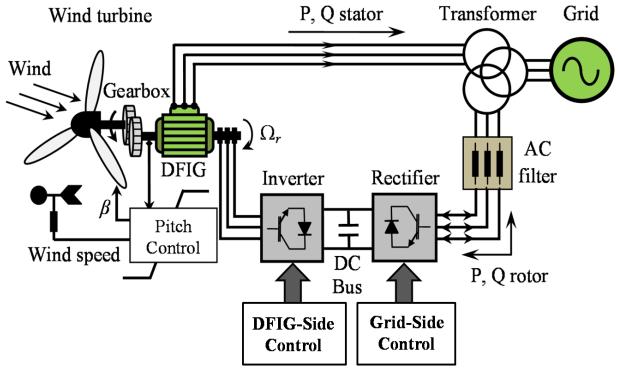

Fig. 1. WECS based a DFIG configuration.

This arrangement provides flexibility of operation in subsynchronous and supersynchronous speeds in both generating and motoring modes (±30% around the synchronous speed). The power inverter needs to handle a fraction (25-30%) of the total power to achieve full control of the generator.

Control of DFIG wind turbine systems is traditionally based on either stator flux oriented control (FOC) [3] or stator voltage oriented control (VOC) [4]. These techniques decouple the rotor current into active and reactive components; control of the active and reactive power is achieved indirectly by controlling the input currents. Some investigations using PI controllers by using FOC that generates reference currents from active and reactive power errors to the inverter or a cascade PI controllers that generate a rotor voltage which has been presented by [5]. Therefore, the conventional PI controllers, because of their simple structures, are still the most commonly used control techniques in power systems, as can be seen in the control of the wind turbines equipped with DFIGs [4-5-6-7]. Unfortunately, tuning the PI controllers is tedious and it might be difficult to tune the PI gains properly due to the nonlinearity and the high complexity of the system. Another main drawback of this regulator is that its performance depends greatly on accurate machine parameters pertaining to the resistances (by warming-up) and inductances (by saturation).

In the last fifteen years, a new technique, based on the Direct Torque Control (DTC) introduced by I. Takahashi in 1986 [8], the Direct Power Control (DPC), was developed and presented in 1998 by T. Noguchi [9] and applied to DFIG in 2006 by L. Xu [10]. DPC is characterized by its fast dynamic response, simple structure and robust response against parameter variations and it does not utilize a rotor current control loops. In the DPC strategy, the active and reactive powers are estimated, using current measurements, and controlled directly with hysteresis controllers and a switching table similar to the one used in DTC applied for AC machines [10-11]. At last, the main characteristics, advantages and disadvantages of both methods are shown and discussed in the results of the simulation tests of a 1.5MW DFIG by using MATLAB/SIMULINK software.

2. Wind turbine model

The relation between the wind speed and mechanic power, delivered by the wind turbine, can be described by the following equation:

$$P_t = \frac{1}{2}\rho \pi R^2 v^3 C_p(\lambda, \beta) \quad (1)$$

$$\lambda = \frac{\Omega_r R}{v} \quad (2)$$

Where:
C_p: power coefficient; λ: relative speed; β: pitch angle (*deg*); R: radius of turbine (*35.25 m*); Ω_r: turbine speed (*rd/s*); v: wind speed (*m/s*); ρ: air density (*1.225 kg.m*$^{-3}$).

For the VSWT, the approximate expression of the power coefficient can be described by the following expression [12]:

$$C_p = f(\lambda, \beta) = C_1\left(\frac{C_2}{\lambda_i} - C_3\beta - C_4\right)\exp\left(\frac{-C_5}{\lambda_i}\right) + C_6\lambda \quad (3)$$

Where:

C_1=0.5176; C_2=116; C_3=0.4; C_4=5; C_5=21; C_6=0.0068.

$$\frac{1}{\lambda_i} = \frac{1}{\lambda + 0.08\beta} - \frac{0.035}{\beta^3 + 1} \quad (4)$$

The electromagnetic torque produced by the turbine is expressed in the following way:

$$T_t = \frac{P_t}{\Omega_r} = \frac{1}{2}\rho \pi R^3 v^2 C_t(\lambda, \beta) \quad (5)$$

Where C_t is the torque coefficient expressed by:

$$C_t = \frac{C_p}{\lambda} \quad (6)$$

Fig. 2 shows the characteristic of the torque coefficient, with a fixed pitch angle β, for the 1.5MW turbine used in this work.

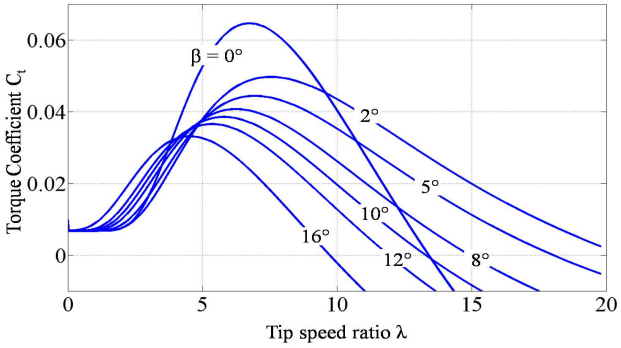

Fig. 2. Pitch angle effect on the torque coefficient.

3. Modeling of the DFIG

In the synchronous *d-q* reference frame rotating at ω_s speed, the model of the DFIG is given by the following equations:
Stator voltage components:

$$\begin{cases} V_{ds} = R_s I_{ds} + \frac{d}{dt}\psi_{ds} - \omega_s \psi_{qs} \\ V_{qs} = R_s I_{qs} + \frac{d}{dt}\psi_{qs} + \omega_s \psi_{ds} \end{cases} \quad (7)$$

Rotor components:

$$\begin{cases} V_{dr} = R_r I_{dr} + \frac{d}{dt}\psi_{dr} - (\omega_s - \omega_r)\psi_{qr} \\ V_{qr} = R_r I_{qr} + \frac{d}{dt}\psi_{qr} + (\omega_s - \omega_r)\psi_{dr} \end{cases} \quad (8)$$

Stator flux components:

$$\begin{cases} \psi_{ds} = L_s I_{ds} + L_m I_{dr} \\ \psi_{qs} = L_s I_{qs} + L_m I_{qr} \end{cases} \quad (9)$$

Rotor flux components:

$$\begin{cases} \psi_{dr} = L_r I_{dr} + L_m I_{ds} \\ \psi_{qr} = L_r I_{qr} + L_m I_{qs} \end{cases} \quad (10)$$

DFIG electromagnetic torque:

$$T_{em} = -\frac{3}{2} p \frac{L_m}{L_r}\left(\psi_{ds} I_{qr} - \psi_{qs} I_{dr}\right) \quad (11)$$

Mechanical equation:

$$T_t = T_{em} + J\frac{d\Omega_r}{dt} + f_r \Omega_r \quad (12)$$

Generator active and reactive powers at the stator side are given by the expressions:

$$\begin{cases} P_s = \frac{3}{2}\left(V_{ds} I_{ds} + V_{qs} I_{qs}\right) \\ Q_s = \frac{3}{2}\left(V_{qs} I_{ds} - V_{ds} I_{qs}\right) \end{cases} \quad (13)$$

3. Field oriented control strategy

The rotor-side converter is controlled in a synchronously rotating *d-q* axis frame, with the *d*-axis oriented along the stator flux vector position (Fig. 3). In this approach, decoupled control between the stator active and reactive powers is obtained. The influence of the stator resistance can be neglected and the stator flux can be held constant as the stator is connected to the grid. Consequently [9]:

$$\psi_{ds} = \psi_s \quad and \quad \psi_{qs} = 0 \quad (14)$$

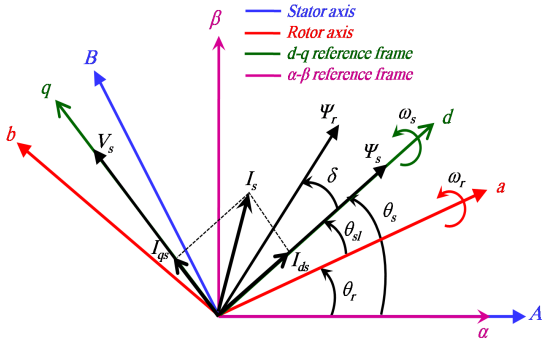

Fig. 3. Stator field oriented control technique.

Since the stator is directly connected to the grid and the stator flux can be considered constant, and if the voltage dropped in the stator resistance has been neglected [5-6], the voltage equations, flux equations, currents equations and stator active and reactive powers equations can be simplified in study state as:

$$\begin{cases} V_{ds} = 0 \\ V_{qs} = V_s = \omega_s . \psi_s \end{cases} \tag{15}$$

$$\begin{cases} \psi_s = L_s I_{ds} + L_m I_{dr} \\ 0 = L_s I_{qs} + L_m I_{qr} \end{cases} \tag{16}$$

$$\begin{cases} I_{ds} = \dfrac{\psi_s}{L_s} - \dfrac{L_m}{L_r} I_{dr} \\ I_{qs} = -\dfrac{L_m}{L_s} I_{qr} \end{cases} \tag{17}$$

$$\begin{cases} P_s = \dfrac{3}{2} V_s I_{qs} \\ Q_s = \dfrac{3}{2} V_s I_{ds} \end{cases} \tag{18}$$

Replacing the stator currents by their expressions given in (17), the equations below are expressed:

$$\begin{cases} P_s = -\dfrac{3}{2} \dfrac{L_m}{L_s} V_s I_{qr} \\ Q_s = \dfrac{3}{2} V_s \left(\dfrac{V_s}{L_s . \omega_s} - \dfrac{L_m}{L_s} I_{dr} \right) \end{cases} \tag{19}$$

The electromagnetic torque is as follows

$$T_{em} = -\frac{3}{2} p \frac{L_m}{L_s} \psi_s I_{qr} \tag{20}$$

Due to the constant stator voltage, the stator active and reactive powers are controlled by means of I_{qr} and I_{dr} respectively. We could express the rotor voltages according to the rotor currents, thus we obtain:

$$\begin{cases} V_{dr} = R_r I_{dr} - g\omega_s \left(L_r - \dfrac{L_m^2}{L_s} \right) I_{qr} \\ V_{qr} = R_r I_{qr} + g\omega_s \left(L_r - \dfrac{L_m^2}{L_s} \right) I_{dr} + g \dfrac{L_m V_s}{L_s} \end{cases} \tag{21}$$

The pole-placement method is used to design PI controllers in current control loops and power control loops [5-6]. Consequently, the resulting overall control system implemented on the DFIG corresponds to the block diagram presented in Fig. 4.

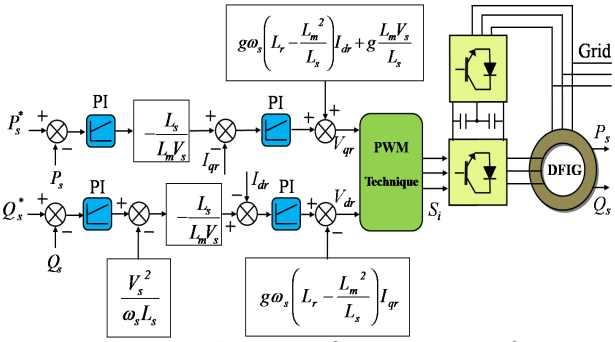

Fig. 4. Schematic diagram of FOC strategy for DFIG.

4. Direct power control strategy

The DPC is based on the same control principles as the DTC technique, the unique difference is the directly controlled variables. In the case of the DTC, the electromagnetic torque and the rotor flux are directly controlled while in the DPC, the stator active and reactive powers are controlled. First a conceptual study of the classical DPC technique will be carried out. In this section, we present the direct control of active and reactive powers by using tow levels voltage source inverter (2L-VSI) which supplies the rotor windings as we show in Fig. 5.

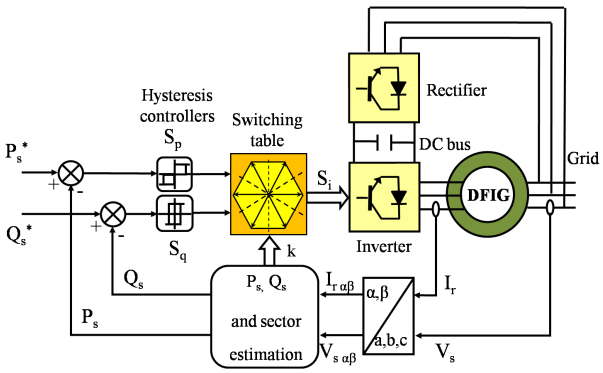

Fig. 5. Schematic diagram of DPC strategy for DFIG.

A. Stator active and reactive power estimation

Instead of measuring the tow powers on the line, we capture the rotor currents, and estimate P_s and Q_s. This approach gives an anticipated control of the powers in the stator windings. By using the stator flux oriented

control and pervious equations presented in section 3 with hypothesis of (R_s=0), we can find the relations of P_s and Q_s according to both components of the rotor flux in the stationary α_r-β_r reference frame, and we can get:

$$\begin{cases} P_s = -\dfrac{3}{2}\dfrac{L_m}{\sigma L_s L_r} V_s \psi_{\beta r} \\ Q_s = \dfrac{3}{2} V_s \left(\dfrac{1}{\sigma L_s} \psi_s - \dfrac{L_m}{\sigma L_s L_r} \psi_{\alpha r} \right) \end{cases} \quad (22)$$

Where:

$$\begin{cases} \psi_{\alpha r} = \left(L_r - \dfrac{L_m^{\,2}}{L_s} \right) I_{\alpha r} + \dfrac{L_m}{L_s} \psi_s \\ \psi_{\beta r} = \left(L_r - \dfrac{L_m^{\,2}}{L_s} \right) I_{\beta r} \\ \psi_r = \sqrt{\psi_{\alpha r}^{\,2} + \psi_{\beta r}^{\,2}} \\ \left| \overline{\psi}_s \right| = \dfrac{\left| \overline{V}_s \right|}{\omega_s} \\ \sigma = 1 - \dfrac{L_m^2}{L_s L_r} \end{cases} \quad (23)$$

If we introducing the flux power angle δ between stator and rotor flux space vectors, P_s and Q_s become:

$$\begin{cases} P_s = -\dfrac{3}{2}\dfrac{L_m}{\sigma L_s L_r} \omega_s |\psi_s| |\psi_r| \sin\delta \\ Q_s = \dfrac{3}{2}\dfrac{\omega_s}{\sigma L_s} |\psi_s| \left(\dfrac{L_m}{L_r} |\psi_r| \cos\delta - |\psi_s| \right) \end{cases} \quad (24)$$

Differentiating (24) results in the following equations:

$$\begin{cases} \dfrac{dP_s}{dt} = -\dfrac{3}{2}\dfrac{L_m \omega_s}{\sigma L_s L_r} |\psi_s| \dfrac{d\left(|\psi_r| \sin\delta \right)}{dt} \\ \dfrac{dQ_s}{dt} = \dfrac{3}{2}\dfrac{L_m \omega_s}{\sigma L_s L_r} |\psi_s| \dfrac{d\left(|\psi_r| \cos\delta \right)}{dt} \end{cases} \quad (25)$$

As we see in (25), these last two expressions show that the stator active and reactive powers can be controlled by modifying the relative angle between the rotor and stator flux space vectors and their amplitudes. This effect is illustrated in the next sections.

B. Switching table

The references of active and reactive powers values are compared with the estimated ones respectively in hysteresis controllers, with S_p and S_q are the outputs signal of active and reactive powers controllers respectively.

We elaborated the switching table of the control structure; according to the outputs of the controllers S_p, S_q and the rotor flux position δ.

For this purpose, the evolution space of ψ_r in the considered reference frame is divided into six sectors; this choice is dictated by preoccupation with a more rigorous control, and such as:

$$-\frac{\pi}{6} + (k-1)\frac{\pi}{3} \le \delta(k) \le \frac{\pi}{6} + (k-1)\frac{\pi}{3} \quad (26)$$

With: $k=1, 2 \ldots 6$

The digitized error signal S_p and S_q and the rotor flux sector are input to the switching table in which every switching state S_a, S_b and S_c of the 2L-VSI is stored as shown in Table 1.

Table 1
Switching table with zero voltage vectors

S_q	1			-1		
S_p	1	0	-1	1	0	-1
Sector 1	V_5	V_7	V_3	V_6	V_0	V_2
Sector 2	V_6	V_0	V_4	V_1	V_7	V_3
Sector 3	V_1	V_7	V_5	V_2	V_0	V_4
Sector 4	V_2	V_0	V_6	V_3	V_7	V_5
Sector 5	V_3	V_7	V_1	V_4	V_0	V_6
Sector 6	V_4	V_0	V_2	V_5	V_7	V_1

C. Rotor active voltage vectors effect on powers

Considering that the stator flux space vector amplitude is constant, the stator active and reactive powers only depend on the relative angle between the fluxes (δ), and the rotor flux space vector amplitude.

Considering anticlockwise direction of rotation of the flux vectors in the rotor reference frame to be positive, it may be noted that ψ_s is ahead ψ_r in motoring mode of operation and ψ_s is behind ψ_r in generating mode [11] (Fig. 6). In the rotor reference frame the flux vectors rotate in the positive direction at subsynchronous speeds, remain stationary at synchronous speed and start rotating in the negative direction at supersynchronous speeds.

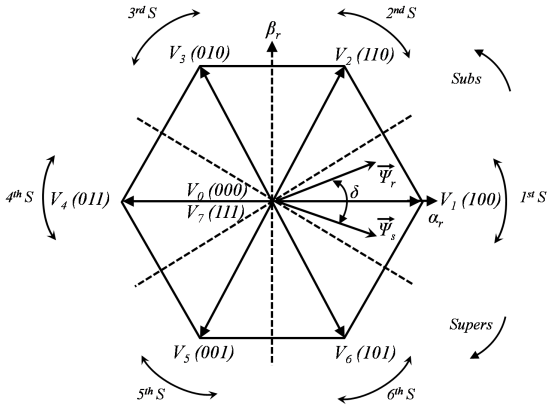

Fig. 6. Flux vectors in rotor coordinates for generating mode.

Assuming that the rotor flux is located in the first sector, the application of voltages vectors V_2 and V_3 results in a decrease in the stator active power whereas, the application of vectors V_5 and V_6 would increase it. In the other hand, the application of V_2 and V_6 would decrease the reactive power drawn from the stator side, while V_3 and V_5 would increase it.

As a generalization it can therefore, be said that if the rotor flux resides in the k^{th} sector, where k = 1, 2, …6, the application of voltage vectors V_{k+1} and V_{k+2} would decrease the delivered stator active power, while the vectors V_{k-1} and V_{k-2} would increase it. Moreover, the application of V_{k+1} and V_{k-1} would decrease (-) the delivered reactive powers, while V_{k+2} and V_{k-2} would increase (+) it, while the zero voltage vectors have a negligeted (0) effect in Q_s. Then, for each sector, only four active vectors are permitted (V_{k-2}, V_{k-1}, V_{k+1}, V_{k+2}) and the zero vectors (V_0, V_7).

The expected direction of change in Q_s due to the application of any switching state in the different sectors can be summarized in Table 2.

Table 2
Expected direction of change in Q_S

	V_0	V_1	V_2	V_3	V_4	V_5	V_6	V_7
Sector 1	0	0	-	+	0	+	-	0
Sector 2	0	-	0	-	+	0	+	0
Sector 3	0	+	-	0	-	+	0	0
Sector 4	0	0	+	-	0	-	+	0
Sector 5	0	+	0	+	-	0	-	0
Sector 6	0	-	+	0	+	-	0	0

In case of discrepancy, the current sector must be updated according to Table 3 [13], by shifting its position clockwise (-1), anticlockwise (+1), or just keeping its previous position (0). The DPC sampling period must be small enough so as to never miss the shift of the rotor flux between two adjacent sectors. It may however, be noted that in a particular sector not all vectors will be applied. For example, in the k^{th} sector, vectors V_k and V_{k+3} will never be applied [14].

Table 3
Sector update table

	V_0	V_1	V_2	V_3	V_4	V_5	V_6	V_7
Sector 1	0	0	-1	+1	0	-1	+1	0
Sector 2	0	+1	0	-1	+1	0	-1	0
Sector 3	0	-1	+1	0	-1	+1	0	0
Sector 4	0	0	-1	+1	0	-1	+1	0
Sector 5	0	+1	0	-1	+1	0	-1	0
Sector 6	0	-1	+1	0	-1	+1	0	0

D. Zero voltage vector effect on powers

Notice that the order of voltage vectors is opposite in subsynchronous operation with respect to supersynchronous operation. The zero voltage vectors V_0 and V_7 stall the rotor flux vector without affecting its magnitude. Their effect on active power is thus opposite in subsynchronous and supersynchronous operation.

In subsynchronous motoring, application of a zero vector increases δ as ψ_s keeps rotating in the positive direction at slip speed. Above the synchronous speed, ψ_s rotates in the anticlockwise direction thereby reducing δ; hence active power drawn by the stator increases for subsynchronous operation and decreases for supersynchronous operation. Active power generated being negative, the same conclusion holds true for the generating modes as well.

Since a zero vector does not change the magnitude of the rotor flux its effect on the reactive power is rather small. Nevertheless, there is some small change in Q_s; its effect being dependent on whether the angle between the stator and rotor fluxes increases or decreases due to the application of a zero vector. An increase (↑) in angular separation between the two fluxes reduces (↓) ψ_{sr} resulting in an increment (↑) of Q_s drawn from the stator side. The converse is true when δ reduces. It is observed that the change in Q_s due to the application of the zero vectors is different in all the 4 modes of operation. This is summarized in Table 4.

Table 4
Zero voltage vector effects on reactive power

Speed	Motoring	Generating
Subs	$\delta\uparrow \Rightarrow \psi_{sr}\downarrow \Rightarrow Q_s\uparrow$	$\delta\downarrow \Rightarrow \psi_{sr}\uparrow \Rightarrow Q_s\downarrow$
Supers	$\delta\downarrow \Rightarrow \psi_{sr}\uparrow \Rightarrow Q_s\downarrow$	$\delta\uparrow \Rightarrow \psi_{sr}\downarrow \Rightarrow Q_s\uparrow$

5. Simulation results

In this part, simulations are investigated with a 1.5MW DFIG connected to a 398V/50Hz grid (appendix), by using the MATLAB/SIMULINK software in fixed-step size of 0.1ms. The both control strategies FOC and DPC are simulated, tested and compared in terms of power reference tracking, robustness against machine parameter variations and stator current harmonics distortion.

1) Power reference tracking: in this test, we initial simulation with various active and reactive powers steps in nominal regime of DFIG with a normal rotor operating speed range (1000 rpm to 2000 rpm) and nominal stator voltage). The active power step is changed from -0.5MW to -1.5MW at the instants t= 0.35s and again from -1MW to -0.5MW at the instant t=0.7s; while the reactive power step is changed from -0.5MVAR to 0.5MVAR at the instant t=0.45s. (The negative sign "-" refers to the generation of active power and to the absorption of reactive power). The simulation results are show in Fig. 7 for the FOC strategy and in Fig. 8 for the DPC strategy.

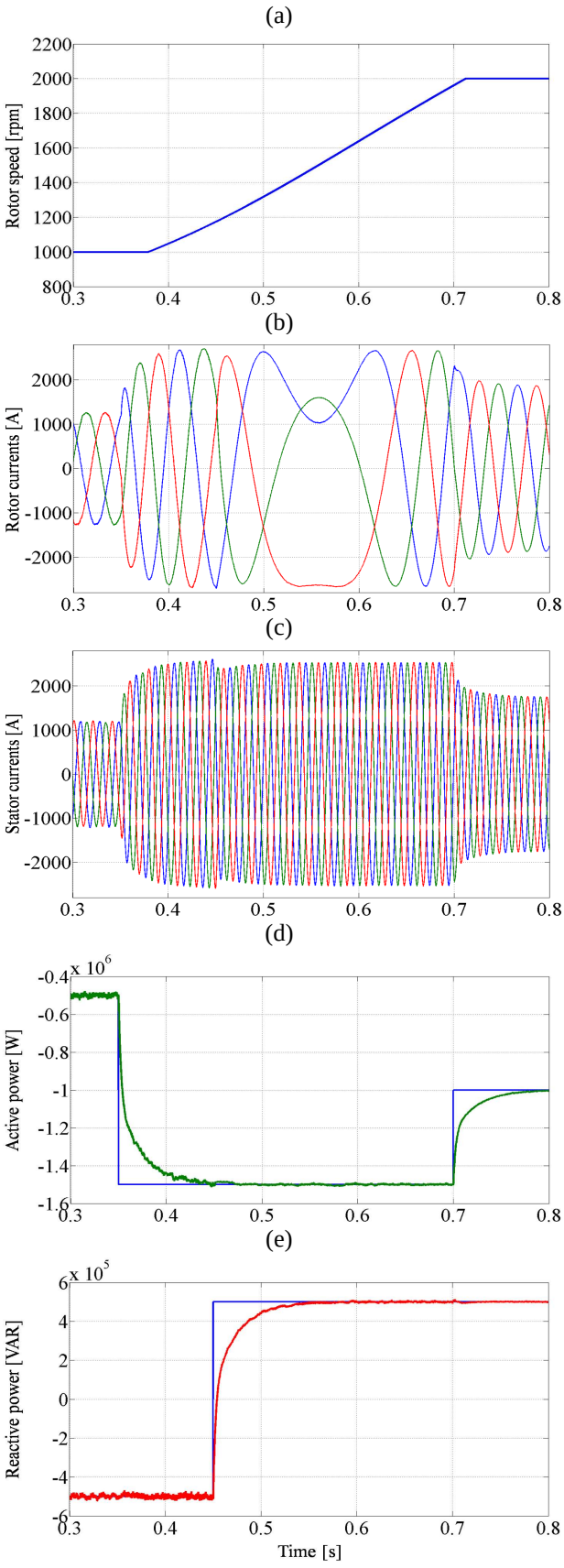

Fig. 7. FOC strategy responses.

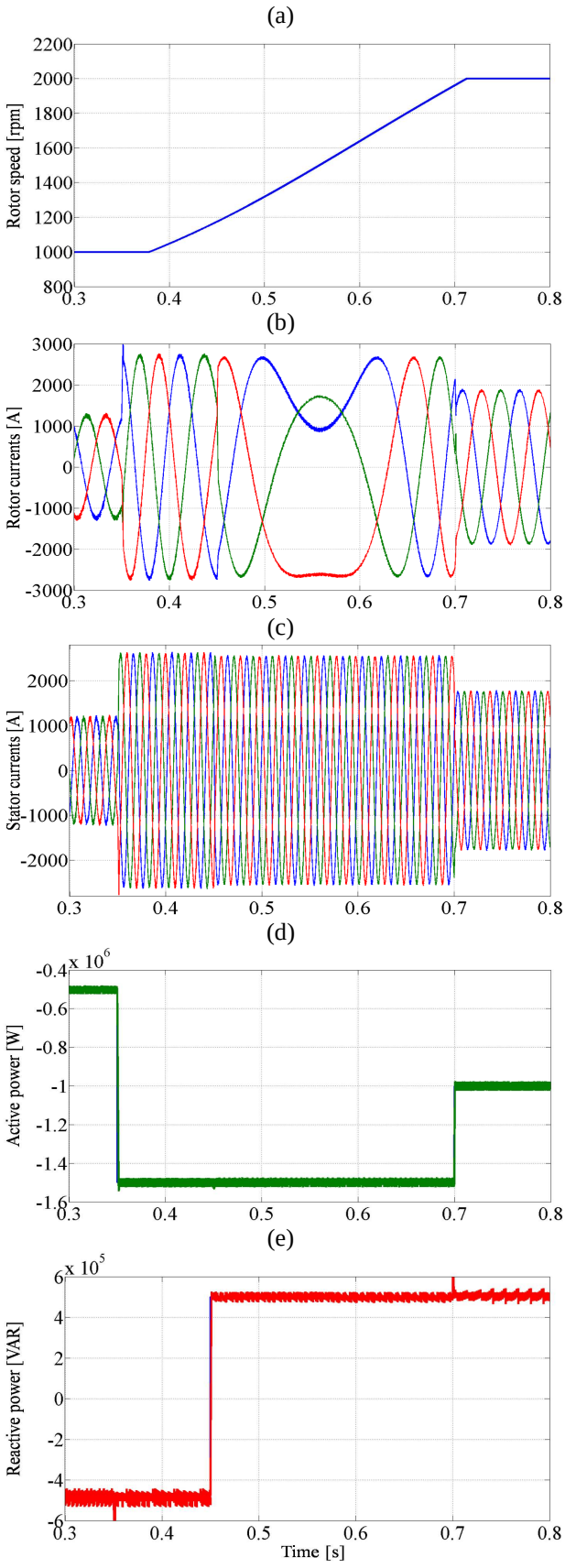

Fig. 8. DPC strategy responses.

The results steps responses in Fig. 7 and Fig. 8 show that the decoupled control of active and reactive power is achieved for both strategies, the tow controllers pursue the references powers, but the DPC strategy show a faster time response (2.13ms for active power and 1.97ms for reactive power) than the FOC strategy (0.09s for active power and 0.08s for reactive power).

2) DFIG parameter variations: to test the impact of parameters variations on the performances of each strategy, we increase the rotor resistance *(R_r)* of 100% (case of warming-up of rotor windings) and decrease the mutual inductance *(L_m)* of 10% (case of inductances saturation). Fig. 9 shows the simulation results.

(a)

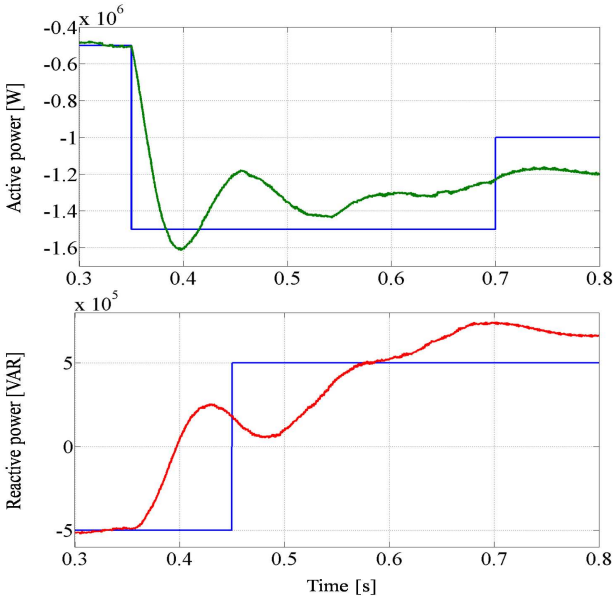

(b)

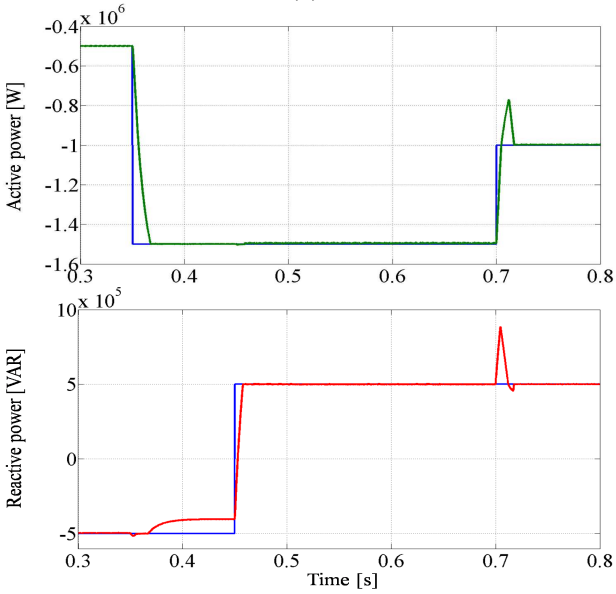

Fig. 9. Both control strategies responses against parameter variations of DFIG: (a) for FOC strategy and (b) for DPC strategy.

Simulation results on Fig. 9-(b) shows the robustness of the DPC strategy against parameter variations of the DFIG especially to the mutual inductance variations; this does not depend on the machine parameters contrary to the FOC strategy [Fig. 9-(a)] that more heavily depends on machine parameters.

3) Current harmonics distortion: in the last test, the reactive power reference will be set to zero (Q_s^*=0 MVAR) to ensure a unity power factor (PF) at the grid side, in order to optimize the generated stator active power quality. In this case the THD rate of the stator current in each strategy cans be evaluated by using the Fast Fourier Transform (FFT); the THD is evaluated for tow cycles. The results are presented in Fig. 10.

(a)

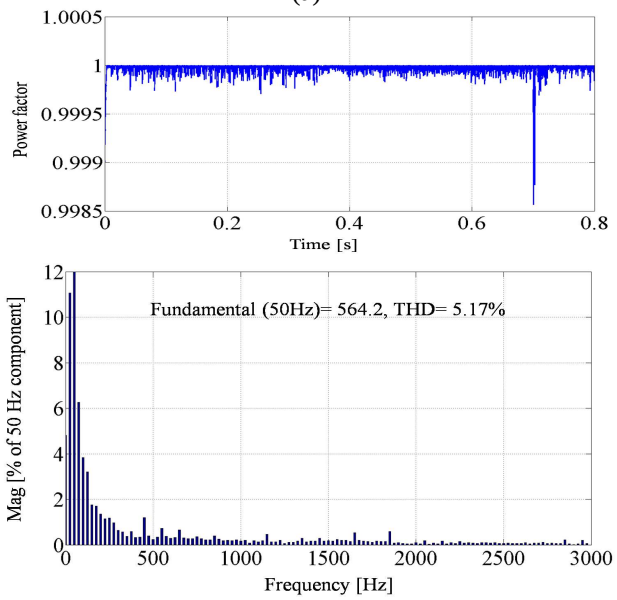

(b)

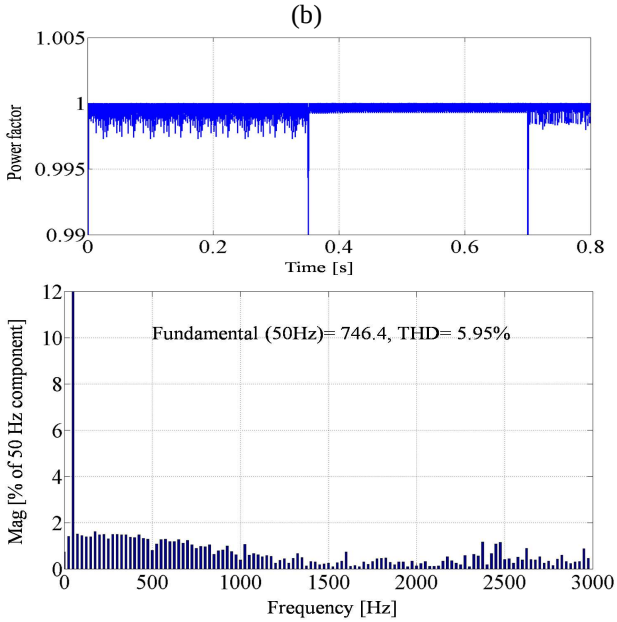

Fig. 10. THD rate, (a) for FOC strategy, (b) for DPC strategy.

On the other hand, unitary power factor at the grid side of DFIG is kept during the transition of the stator current both in FOC strategy [Fig. 10-(a)] and DPC strategy [Fig. 10-(b)]; while $Q_s^* = 0$ and P_s is varied.

The current harmonic distortion test of the tow strategies presented in Fig. 10 shows that the harmonics rate in the case of the DPC strategy [Fig. 10-(b)] is more significant (5.95%) than those in the case of the FOC strategy, which is only 5.17% [Fig. 10-(a)], and it's due to the use of hysteresis controllers and the switching table in the first one witch result in the variable switching frequency.

Finally, the Table 5 summaries the principal differences between the FOC strategy and the DPC strategy.

Table 5
Comparison of FOC and DPC schemes

	FOC	DPC
Computational complexity	High	Low
Machine model dependency	High	Low
Sample time constraints	Low	High
Transitory response	Medium	Very good
Harmonic currents	Low	Medium
Overall implementation complexity	High	Medium
Robustness	Low	Medium
PWM	Required	Not required
Coordinates reference frame	*d-q* reference frame	*α-β* reference frame
Controllers	Four PI controllers	Tow hysteresis controllers
Switching frequency	Constant	Variable
Active and reactive power control	Indirectly controlled by rotor currents	Directly controlled

6. Conclusions

This paper has presented a comparative study between two control strategies of active and reactive powers for Doubly Fed Induction Generator, the: FOC and DPC. The first one is based on PI controllers and the second one on hysteresis controllers and a switching table. So as to evaluate the performances of each strategy, we have put the two strategies under various conditions such as: changing powers steps references, and parameters variations of the DFIG.

The comparisons of simulation results between tow strategies show that for both strategies the decoupled of active and reactive power is achieved. But, in steady state of DFIG, the DPC strategy presents a high dynamic response, and it's more robust against parameters variation of the DFIG.

However this strategy because of the variable switching frequency presents the drawback to having a high frequency of switching which present a high harmonic distortion of the generated currents, high ripples of active and reactive powers, and warming-up of the silicon switchers compared to the FOC strategy.

Then, the big criterion to engineers and researches is to choose between both strategies mainly the requirements of the application in terms of high performances in ideal conditions and robustness in the case of parameters variations, involved in the field of DFIG based wind energy conversion systems.

Appendix

Table 6
Wind turbine parameters

Blade radius, R	35.25 m
Number of blades	3
Gearbox ratio, G	90
Moment of inertia, J	1000 Kg.m^2
Viscous friction coefficient, f_r	0.0024 N.m.s^{-1}
Cut-in wind speed	4 m/s
Cut-out wind speed	25 m/s
Nominal wind speed, v	16 m/s

Table 7
Doubly fed induction generator parameters

Rated power, P_n	1.5 MW
Stator rated voltage, V_s	398/690 V
Rated current, I_n	1900 A
Rated DC-Link voltage U_{DC}	1200 V
Stator rated frequency, f	50 Hz
Stator inductance, L_s	0.0137 H
Rotor inductance, L_r	0.0136 H
Mutual inductance, L_m	0.0135 H
Stator resistance, R_s	0.012 Ω
Rotor resistance, R_r	0.021 Ω
Number of pair of poles, p	2

References

1. A. Petersson, "*Analysis, modeling and control of doubly fed induction generators for wind turbines*", PhD. thesis, Champers University of Technology, Sweden, 2005.
2. S. EL Aimani, B, François, F. Minne, and B. Robyns, "*Modelling and simulation of doubly fed induction generators for variable speed wind turbines integrated in a distribution network*", 10th European conference on power electronics and applications, Toulouse, France, 2–4 September 2003.
3. B. Hopfensperger, D. J. Atkinson, and R. Lakin, "*Stator-flux-oriented control of a doubly-fed induction machine with and without position encoder*", IEE Proc.-Electr. Power Applications, vol. 147, no. 4, July 2000, pp. 241-250.

4. Y. Zhou, P. Bauer, J.A. Ferreira, and J. Pierik, "*Control of DFIG Under Unsymmetrical Voltage Dip*", IEEE Power Electronics Specialists Conference, 2007, pp. 933-938.
5. A. Tapia, G. Tapia, J. X. Ostolaza, and J. R. Sáenz, "*Modeling and control of a wind turbine driven doubly fed induction generator*", IEEE Trans. on Energy Conversion, June 2003, pp. 194–204.
6. G. Tapia, A. Tapia, and J. X. Ostolaza, "*Proportional–integral regulator based approach to wind farm reactive power management for secondary voltage control*", IEEE Trans. Energy Conversion, vol. 22, no. 2, June 2007, pp. 488-498.
7. M. Yamamoto, O. Motoyoshi, "*Active and reactive power control for doubly-fed wound rotor induction generator*", IEEE Transactions on Power Electronics, vol. 6, no. 4, October 1991, pp. 624-629.
8. I. Takahashi and T. Noguchi, "*A new quick-response and high-efficiency control strategy of an induction motor*", IEEE Trans. Ind. Appl., vol. IA-22, no. 5, October 1986, pp. 820-827.
9. T. Noguchi, H. Tomiki, S. Kondo, and I. Takahashi, "*Direct power control of PWM converter without power-source voltage sensors*", IEEE Trans. Ind. Applications., vol. 34, May/June 1998, pp. 473–479.
10. L. Xu, P. Cartwright, "*Direct active and reactive power control of DFIG for wind energy generation*", IEEE Trans. Energy Conversion, vol. 21, no. 3, Sept 2006, pp.750-758.
11. R. Datta, V. T. Ranganathan, "*Direct power control of grid-connected wound rotor induction machine without rotor position sensors"*, IEEE *Trans. Power Electron*, vol. 16, no. 3, May 2001, pp. 390-399.
12. S. Heier, Grid *Integration of Wind Energy Conversion Systems*, John Wiley & Sons, 2006.
13. E. Tremblay, S. Atayde, and A. Chandra, "*Comparative study of control strategies for the doubly fed induction generator in wind energy conversion systems: A DSP-based implementation approach*", IEEE Trans. Sustainable Energy, vol. 2, no. 3, July 2011, pp. 288-299.
14. G. Abad and all, *Doubly Fed Induction Machine: Modeling and Control for Wind Energy Generation*, Institute of Electrical and Electronic Engineers, Inc. Published by John Wiley & Sons, Inc, 2011.